APL Photonics

RESEARCH ARTICLE | JUNE 16 2023

Kerr nonlinearity and group velocity dispersion of InGaAs/InP and GaAsSb/InP waveguides in the mid-infrared

Kevin Zhang ✉; Gerhard Böhm; Mikhail A. Belkin ✉

APL Photonics 8, 066107 (2023)
https://doi.org/10.1063/5.0151013

Kerr nonlinearity and group velocity dispersion of InGaAs/InP and GaAsSb/InP waveguides in the mid-infrared

Cite as: APL Photon. 8, 066107 (2023); doi: 10.1063/5.0151013
Submitted: 17 March 2023 • Accepted: 4 June 2023 •
Published Online: 16 June 2023

Kevin Zhang,[a] Gerhard Böhm, and Mikhail A. Belkin[a]

AFFILIATIONS

Walter Schottky Institute, Technical University of Munich, Garching 85748, Germany

[a]Authors to whom correspondence should be addressed: kevin.zhang@wsi.tum.de and mikhail.belkin@wsi.tum.de

ABSTRACT

We report measurements of Kerr nonlinearity and group velocity dispersion in $In_{0.53}Ga_{0.47}As$/InP and $GaAs_{0.51}Sb_{0.49}$/InP ridge waveguides in the mid-infrared using four-wave mixing at $\lambda \approx 5\ \mu$m. Measured values of Kerr nonlinearity are significantly higher compared to those reported for any other materials systems suitable for building dielectric waveguides with low losses and low group velocity dispersion in the mid-infrared ($\lambda \approx 3$–$15\ \mu$m). Our measurements establish both $In_{0.53}Ga_{0.47}As$/InP and $GaAs_{0.51}Sb_{0.49}$/InP materials as promising platforms for the development of on-chip mid-infrared frequency comb generation and supercontinuum light sources.

Compact chip-scale mid-infrared (mid-IR, $\lambda \approx 3$–$15\ \mu$m) light sources that are bright, broadband, and can be produced at low cost in mass quantities are highly desired for spectroscopic applications in the molecular fingerprint region. Compared to thermal sources, laser-based mid-IR supercontinuum and frequency comb sources can offer orders of magnitude higher spectral brightness, which is needed for many spectroscopic and imaging applications including spectroscopy of biochemical samples in water, high-resolution spectroscopy, high-speed spectroscopy, and spectroscopic imaging with high spatial resolution.[1–4] Direct frequency comb generation inside of mid-IR quantum cascade (QCLs) and interband cascade lasers (ICLs) has been demonstrated;[5–8] however, the bandwidth of these frequency combs is currently limited to ~100 cm^{-1} by the difficulty of maintaining a flat gain profile and managing the group velocity dispersion in the laser waveguides.[5–9] In parallel, octave-spanning Kerr frequency comb generation in passive micro-ring resonators[10–13] has been experimentally demonstrated in the near-infrared spectral range ($\lambda < 3\ \mu$m), and similar approaches are being explored in the 3–5 μm spectral range using SiN- and Si-based micro-ring resonators.[14,15] Additionally, on-chip supercontinuum generation in SiN, Si, and SiGe-based waveguides has been shown to be able to extend the spectral bandwidth of pulsed mid-IR sources to an optical octave or more.[16–18]

Materials transparency, significant Kerr nonlinearity (n_2), and low group velocity dispersion are the three critical parameters that determine the required optical powers for frequency comb and supercontinuum generation. In addition to SiN-, Si- and SiGe-based materials platforms that have been reported for chip-scale frequency comb and supercontinuum generation,[5–8,16–18] the InP-based materials platform is very promising since it provides low optical loss[19] and low group velocity dispersion[5] in the entire mid-IR spectral range and can be seamlessly integrated with mid-IR QCL pumps.[20] However, the value of Kerr nonlinearity in InP-based waveguides has not yet been characterized in the mid-IR spectral range.

Here, we report experimental measurements of n_2 nonlinearity in InP-based mid-IR optical waveguides with the waveguide cores made of $In_{0.53}Ga_{0.47}As$ and $GaAs_{0.51}Sb_{0.49}$ compounds, both are lattice-matched to InP. InGaAs/InP and GaAsSb/InP waveguides represent two possible passive mid-IR waveguiding platforms that can be grown epitaxially on InP and that are compatible with the monolithic integration of QCL pumps. Experimental

measurements performed at $\lambda \approx 5\ \mu m$ give the values of $|n_2| \approx 4.8 \times 10^{-17}\ m^2/W$ and $|n_2| \approx 8.5 \times 10^{-17}\ m^2/W$ for TE-polarized modes in $In_{0.53}Ga_{0.47}As/InP$ and $GaAs_{0.51}Sb_{0.49}/InP$ waveguides, respectively, all grown on [001] InP. These values of Kerr nonlinearity are approximately an order of magnitude higher than those reported for Si-based waveguides and several times higher than those reported for Ge-based waveguides in the mid-IR.[21–25]

The value for n_2 is experimentally measured through the characterization of four wave mixing (FWM) inside passive $In_{0.53}Ga_{0.47}As/InP$ and $GaAs_{0.51}Sb_{0.49}/InP$ ridge waveguides pumped with two closely-spaced laser frequencies ω_1 and ω_2 ($\omega_1 > \omega_2$) centered around $\lambda \approx 5\ \mu m$. The device wafers were grown by molecular beam epitaxy (MBE). For InGaAs samples, a 1.5 μm-thick layer of nominally undoped $In_{0.53}Ga_{0.47}As$ was grown atop an iron-doped semi-insulating (SI) InP substrate followed by a 3 μm-thick layer of nominally undoped InP upper cladding. For GaAsSb samples, a 2 μm-thick layer of nominally undoped $GaAs_{0.51}Sb_{0.49}$ was grown atop an identical iron compensated semi-insulating InP substrate. The GaAsSb waveguide sample did not have a semiconductor upper cladding. The background doping in the nominally undoped layers was approximately $n = 7 \times 10^{14}\ cm^{-3}$, $n = 7 \times 10^{15}\ cm^{-3}$, and $n = 5 \times 10^{15}\ cm^{-3}$ for $In_{0.53}Ga_{0.47}As$, $GaAs_{0.51}Sb_{0.49}$, and InP materials, respectively, based on Hall-effect measurements of similar samples grown previously in the same reactor.

Epitaxial layer thicknesses and waveguide geometries were chosen in order to achieve a near-zero, anomalous group velocity dispersion (GVD) in the 4–6 μm wavelength range. The phase mismatch in a FWM process is directly related to the GVD of the waveguide at the pump wavelength. This property allows us to experimentally determine the GVD of the waveguide by observing the oscillations of the FWM signal intensity as a function of pump frequency, as discussed further later.

For our experiments, the frequency ω_{FWM} generated in a FWM process is given by the expression

$$\omega_{FWM} = 2\omega_1 - \omega_2, \tag{1}$$

where $\omega_2 = \omega_1 - \Delta\omega$ and $\omega_{FWM} = \omega_1 + \Delta\omega$. The phase mismatch is then given by[26]

$$\Delta k = 2k_1 - k_{FWM} - k_2 = \Delta\omega^2 \cdot D_\lambda \frac{\lambda^2}{2\pi c}, \tag{2}$$

where $k_i = \frac{\omega_i}{c} n(\omega_i)$, $D_\lambda = -\frac{\lambda}{c}\frac{\partial^2 n}{\partial \lambda^2} = -\frac{2\pi c}{\lambda^2}\frac{\partial^2 k}{\partial \omega^2}$ is the group velocity dispersion parameter, and λ is the free-space wavelength of the ω_1 pump.

In order to reduce phase mismatch and achieve a measurable amount of FWM using low-power pumping (provided by tunable QCLs), the group velocity dispersion of the waveguides must be minimized. To that end, the waveguides were fabricated with 3 and 8 μm ridge widths for InGaAs and GaAsSb samples, respectively. The schematics of the waveguide cross section and the computed waveguide modes are shown in Fig. 1. Waveguides of different lengths in the range of 1.2–5.1 cm were fabricated from each of the wafers. To clearly discriminate the laser power coupled into the waveguide modes, all the waveguides had a 90° bend with a large bending radius of 300 μm (that produces negligible bending loss).[19] The computed mode intensity distribution for the fundamental TE polarized mode at $\lambda = 5.2\ \mu m$ for both InGaAs and GaAsSb waveguides is shown in Fig. 1. The values for the refractive index of our materials as well as the simulated effective indices and the group velocity dispersion parameters of each waveguide for fundamental TE-polarized modes are shown in Fig. 2. We note that both of our waveguides are expected to have a slight anomalous dispersion in the range of wavelengths used for the experimental testing. This anomalous dispersion often serves to compensate for nonlinear cross-phase and self-phase modulation in microresonator samples that arise proportionally to pump power.[27]

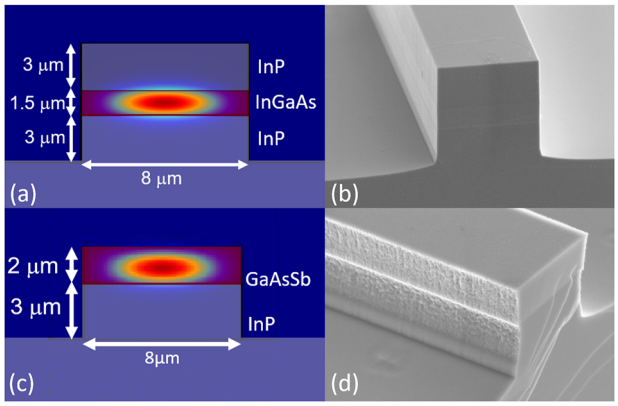

FIG. 1. Scanning electron microscope images of the ridge waveguides used for the experiments and the computed mode intensity distribution for the fundamental TE polarized mode at $\lambda = 5.2\ \mu m$ for (a) and (b) 3 μm-wide InGaAs and (c) and (d) 8 μm-wide GaAsSb waveguides.

Waveguide structures were defined by electron beam lithography. The pattern was then transferred into a Si_xN_y hard mask using CF_4/O_2 based chemistry in an inductively coupled plasma reactive ion etching (ICP-RIE) system. Finally, this pattern was transferred into the semiconductor layer structure using a CH_4/H_2 based chemistry in an ICP-RIE. The residual Si_xN_y hard mask was removed using the same CF_4/O_2 ICP-RIE. The waveguides were then dipped into a solution of $HBr:HNO_3:H_2O$ (1:1:10) for 1 min and $HCl:H_2O$ (1:5) for 30 s to remove residual polymer deposition as a result of the ICP-RIE process and clean any surface oxide, respectively.[19] Waveguide facets were cleaved to expose input and output facets for light in- and out-coupling. A multilayer antireflection coating consisting of YF_3 and ZnS layers was evaporated onto the output facet of the sample to suppress the Fabry–Perot resonances of the waveguides.

The experimental setup used is shown in Fig. 3. Samples were mounted onto a temperature-controlled stage and stabilized to 20 °C. Light outputs from a fixed-frequency single mode distributed feedback (DFB) QCL ($\lambda_1 = 5.2\ \mu m$) and from a broadly tunable QCL laser system ($\lambda_2 = 5.35–6\ \mu m$) were combined using a dichroic mirror and were both coupled to the fundamental transverse electric (TE) mode of the waveguides through the input facet using a lens with a numerical aperture (NA) of 0.85 following the approach described in Ref. 19. Light from the output facet of the waveguide was collected and collimated using a lens pair and then focused onto a calibrated nitrogen cooled InSb photodetector. Short pass filters and one long pass filter positioned in front of the detector were

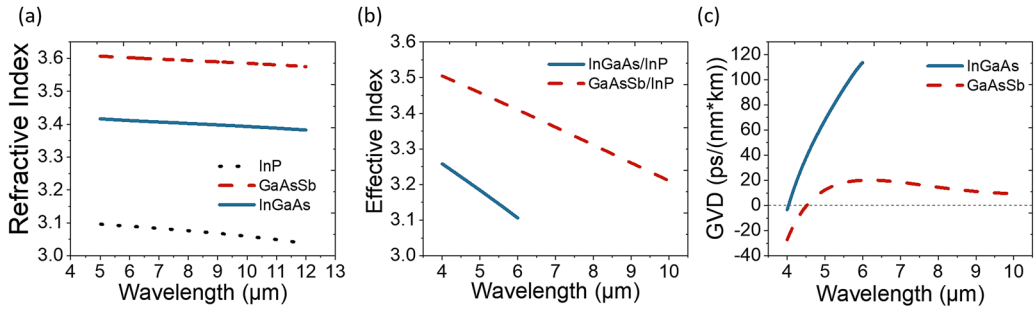

FIG. 2. (a) Mid-IR refractive indices of InP, $In_{0.53}Ga_{0.47}As$, and $GaAs_{0.51}Sb_{0.49}$ materials. The values of refractive indices are obtained by broadband mid-IR measurements of the reflectance of films of these materials on InP. (b) Simulated effective refractive index and (c) group velocity dispersion parameter of the 3 μm-wide InGaAs and 8 μm-wide GaAsSb waveguides used in the experiment.

used to provide a narrow λ_2 = 4.75–5.05 μm transmission window to block the laser's light and its second harmonics to ensure measurement of only light generated via the FWM process. The tunable QCL was tuned in the range of 5.35–5.85 μm, and the resulting FWM power output from the waveguide was measured as a function of the frequency detuning $\Delta\omega$ between the two laser pumps.

The nonlinear power generated in a FWM process inside a waveguide of length L with the intensity attenuation coefficients α_1, α_2, and α_{FWM} for pump 1, pump 2, and the FWM signal can be computed using the following expression:[28]

$$P_{FWM} = \frac{9\omega_{FWM}^2 \chi_{eff}^{(3)^2}}{16 n_{eff}^4 \varepsilon_o^2 c^4} \frac{P_1^2 P_2}{A_{eff}^2} \left[\frac{1 - e^{-\alpha L}[2\cos(\Delta k L)] + e^{-2\alpha L}}{\Delta k^2 + \alpha^2} \right] \times e^{-\alpha_{FWM} L}, \quad (3)$$

where $\alpha = \alpha_1 + \frac{\alpha_2}{2} + \frac{\alpha_{FWM}}{2}$, $A_{eff} = \frac{(\int |E|^2 dA)^2}{\int |E|^4 dA}$ is the effective area of the four wave interaction in the waveguide[29] (assuming all mode areas are approximately the same for all the wavelengths involved in the process), n_{eff} is the effective refractive index, $\chi_{eff}^{(3)}$ is the effective nonlinearity for the FWM process in a zinc-blende semiconductor with

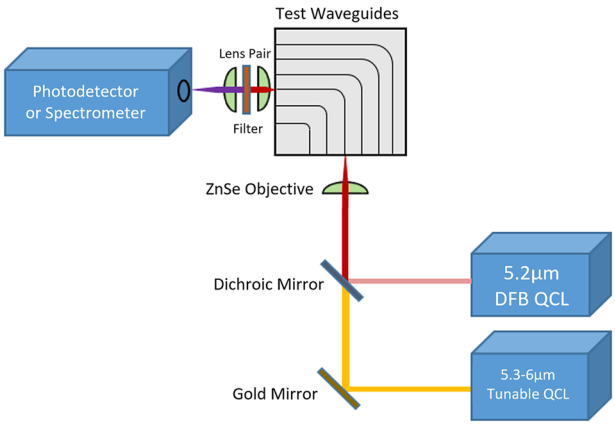

FIG. 3. Experimental setup used to measure degenerate four wave mixing.

the electric field vectors oriented in the x–y plane of the semiconductor principle coordinate system, and P_i is the power of pump i (i = 1, 2) coupled into the waveguide input facet. The values of P_i are determined by measuring the laser power output from the waveguides using a calibrated thermopile detector and by correcting the measured values for the collection efficiency of the setup and for the measured waveguide propagation losses (the latter are determined in a manner similar to that described in Ref. 19 using waveguides with uncoated facets). Typical spectra of the pump, idler, and FWM signals are shown in Fig. 4(c).

Figure 4 displays the FWM conversion efficiency defined as

$$\eta = \frac{P_{FWM}}{P_1^2 P_2} = \frac{9\omega_{FWM}^2 \chi_{eff}^{(3)^2}}{16 n_{eff}^4 \varepsilon_o^2 c^4} \frac{1}{A_{eff}^2} \left[\frac{1 - e^{-\alpha L}[2\cos(\Delta k L)] + e^{-2\alpha L}}{\Delta k^2 + \alpha^2} \right] \times e^{-\alpha_{FWM} L}, \quad (4)$$

measured as a function of frequency detuning $\Delta\omega$ between the two laser pumps. The dependence of the conversion efficiency on $\Delta\omega$ was fitted using Eq. (4) to determine $\chi_{eff}^{(3)^2}$, Δk, $\Delta\alpha$, and D_λ. The waveguide loss at the FWM frequency was approximated to be α_{FWM} ≈ 0.5 dB/cm for InGaAs based upon our previous waveguide loss measurements of the same materials[19] between λ = 5–6 μm and noting that the losses of a 3 μm wide ridge stay relatively constant within that range. Waveguide loss for GaAsSb was measured using the same method described in Ref. 19, giving a value of approximately α_{FWM} ≈ 3 dB/cm at 5.2 μm. This was approximated to also be close to the real value of the loss at the FWM frequency. The length of measured waveguides was L_{InGaAs} = 1.65 cm and L_{GaAsSb} = 1.25 cm; the value of refractive index used was extracted from Fig. 2 ; and the effective mode areas used were $A_{ef\,f_{InGaAs}} = 4.7 \times 10^{-12}$ m^2 and $A_{ef\,f_{GaAsSb}} = 9.9 \times 10^{-12}$ m^2. Equation (4) predicts the oscillatory behavior of the FWM output as a function of $\Delta\omega$ as confirmed by experiment in the case of InGaAs waveguides [Fig. 4(a)]. Due to the near-zero GVD of the GaAsSb sample as well as the limited tuning range of the idler laser, the detuning $\Delta\omega$ attainable in our experiment was not sufficient to observe FWM power oscillations in that sample [Fig. 4(b)]. As a result of the fitting, we determine the D_λ for the InGaAs/InP and GaAsSb/InP waveguide structures at λ = 5.2 μm to be ~68 ± 10 and 17 ± 1 $\frac{ps}{nm\ km}$, respectively, in close

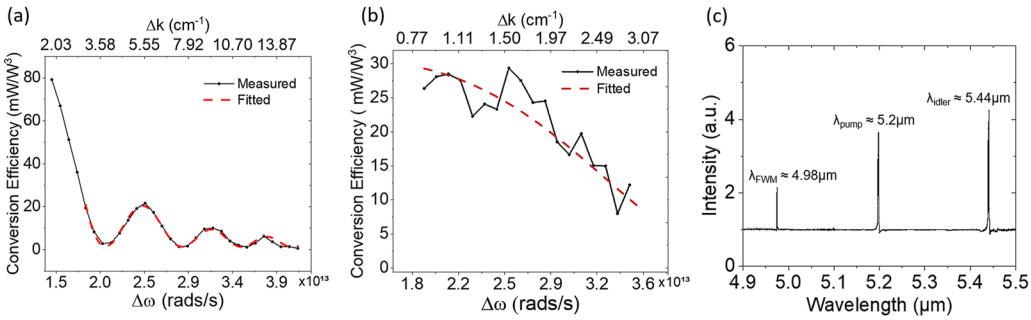

FIG. 4. Measured FWM conversion efficiency as well as fit function based on Eq. (4) for InGaAs (a) and GaAsSb (b) waveguides. (c) Measured transmission spectra of an InGaAs waveguide with $\lambda_{idler} = 5.44\ \mu m$. The FWM line spectrum was obtained using interference filters to block the much stronger signal and idler lines and is not to scale with the spectra of the signal and idler.

agreement with our simulation results shown in Fig. 2. We further calculate the value of $|\chi_{eff}^{(3)}|$ to be $1.7 \times 10^{-18}\frac{m^2}{V^2}$ and $3.3 \times 10^{-18}\frac{m^2}{V^2}$ for InGaAs/InP and GaAsSb/InP waveguides, respectively. Away from material resonances, $\chi_{eff}^{(3)}$ is a real number, and then the value of the Kerr nonlinearity, n_2, and $|\chi_{eff}^{(3)}|$ are directly related by the following expression:[28]

$$n_2 = \frac{3\chi^{(3)}}{4\epsilon_o c n^2}. \tag{5}$$

Using Eq. (5), we obtain the value of the Kerr nonlinearity for our InGaAs/InP and GaAsSb/InP waveguides to be $|n_2| \approx 4.8 \times 10^{-17}$ m^2/W and $|n_2| \approx 8.5 \times 10^{-17}$ m^2/W, respectively, for our experimental configuration. These values of n_2 represent the effective n_2 of the waveguide structure. However, we re-compute the nonlinear overlap integral A_{eff}, as defined in Eq. (3), of the four interacting optical modes within only the InGaAs and GaAsSb waveguide cores and obtain that the core material contributes ~93% and ~99% of the measured n_2 coefficient for the mode, respectively. Additionally, the value of n_2 for InP has been measured in the mid-IR by others, as shown in Table I. Using these nonlinear overlap integral values and assuming the n_2 value for InP shown in Table I is also valid at $\lambda \approx 5.2\ \mu m$, we obtain an adjusted value of the n_2 coefficient for InGaAs to be $|n_2| \approx 5 \times 10^{-17}$ m^2/W, while the GaAsSb value of n_2 remains effectively equivalent to the measured value.

The calibration of the InSb detector was carried out using identical laser power and configuration as used for the measurements in order to minimize errors due to calibration. The primary source of experimental error is expected to be due to the collection efficiency at the output of the waveguide, which will proportionally scale the nonlinear conversion efficiency. However, experimental verification of pump powers at the output facet measured with and without the 0.85 NA collimation lens indicates a near 100% collection efficiency of the collimation lens. Pump powers at the output of the sample were measured after collimation using a thermopile with an area much larger than the far-field profile of the waveguide after collimation, while the nonlinear signal is additionally focused with a 0.5 NA lens and measured with an InSb detector with an area of 1 mm^2.

We note that, aside from the FWM process described earlier, light output at frequency $2\omega_1 - \omega_2$ can also be generated through cascaded three-wave mixing processes that consist of second harmonic generation (SHG) of the light at $2\omega_1$ followed by a difference-frequency generation (DFG) process $2\omega_1 - \omega_2$ or by a DFG process $\omega_1 - \omega_2$ followed by a sum-frequency generation process $\omega_1 - \omega_2 + \omega_1$.[30] We exclude the first possibility by experimentally measuring SHG output at $2\omega_1$ from the waveguide facet. Because of the lack of SHG phase matching in our waveguides, we measured the SHG conversion efficiency (defined as the ratio of SHG power to the product of ω_1 pump power) to be smaller than $1\frac{\mu W}{W^2}$. In order to generate a signal at frequency ω_{FWM}, the SHG photons would then need to undergo a DFG process with the ω_2 beam. By reciprocity in transparent nonlinear materials,[28] this DFG process is expected to have nearly the same second order nonlinearity $\chi_{eff}^{(2)}$ and phase mismatch Δk as the SHG process. As a result, a similar conversion efficiency should be expected for the DFG process, which will result in a conversion efficiency in the cascaded three-wave mixing process of $1\frac{pW}{W^3}$, many orders of magnitude smaller than that produced by the direct FWM. We further exclude contributions from the cascaded three wave mixing process in which we first generate a DFG

TABLE I. Various mid-infrared compatible materials and their corresponding nonlinear refractive indices measured at, or extrapolated to, the indicated wavelength. The data are taken from Refs. 21, 31–33, 36, 38, and 39. The values of n_2 for the SiGe alloys are dependent on the alloy composition and are between those of Si and Ge, as discussed in Ref. 21.

Material	n_2 (10^{-18} m^2/W)	λ (μm)
Si_3N_4	0.24[31]	1.5
As_2Se_3	2.5[32]	1.064
Si	3.26[21]	4.26
$GeSe_4$	3.2[32]	1.55
GaAs	10[33]	2.5
$Ge_{11.5}As_{24}Se_{64.5}$	2.45[38]	4
$Al_{0.32}Ga_{0.68}As$	9[36]	3.06
Ge	25.5[21]	4.26
InP	24[39]	3.9
$In_{0.53}Ga_{0.47}As$ (this work)	50	5.2
$GaAs_{0.51}Sb_{0.49}$ (this work)	85	5.2

wave because our waveguides cannot provide mode confinement at frequencies $\omega_1 - \omega_2$.

The measured values of n_2 for $In_{0.53}Ga_{0.47}As$ and $GaAs_{0.51}Sb_{0.49}$ materials in the mid-IR compare favorably with Kerr nonlinearities reported in other materials systems suitable for mid-IR photonics integration. Table I summarizes the values of Kerr nonlinearities reported for various mid-IR-transparent materials,[21,31–34] including the results of this work. The waveguide materials studied here possess significantly larger Kerr nonlinearities compared to all the others listed in the table. In particular, they are a factor of 2-3 higher than that reported for the Si and SiGe waveguides in the mid-IR.[21–25] Finally, we note that the measured values of n_2 for $In_{0.53}Ga_{0.47}As$ and $GaAs_{0.51}Sb_{0.49}$ are consistent with the reported value of n_2 for $Al_{0.32}Ga_{0.68}As$ at $\lambda \approx 1.5\ \mu m$[34–36] and the expected $\sim (\frac{1}{E_g})^4$ scaling of n_2 nonlinearity in the transparency region of III-V semiconductors.[28,37] High Kerr nonlinearity, low broadband mid-IR GVD achievable in the $In_{0.53}Ga_{0.47}As$/InP and $GaAs_{0.51}Sb_{0.49}$/InP waveguides, low optical losses,[19] and the possibility of monolithic integration of mid-IR QCL pumps[20] make these materials platforms promising for the development of chip-scale electrically-pumped mid-IR frequency comb and supercontinuum light sources.

In conclusion, we report the characterization of effective Kerr nonlinearity in both the $In_{0.53}Ga_{0.47}As$ and $GaAs_{0.51}Sb_{0.49}$ materials systems at $\lambda \approx 5.2\ \mu m$. The values of $|n_2|$ are found to be $\sim 5 \times 10^{-17}$ and 8.5×10^{-17} m^2/W for InGaAs and GaAsSb materials, respectively. Both of these materials systems provide a Kerr nonlinearity that is significantly larger than that reported for other mid-IR photonic platforms, including GaAs and Si/SiGe. In addition, we experimentally verified the possibility of fabricating ridge waveguides in these materials with near zero values of GVD in the mid-IR.

This work was supported by the EC| H2020 | H2020 Industrial Leadership (IL) PASSEPARTOUT project under Grant No. 101016956 and by the German Research Foundation (DFG) under Grant No. 463411319.

AUTHOR DECLARATIONS

Conflict of Interest

The authors have no conflicts to disclose.

Author Contributions

Kevin Zhang: Data curation (lead); Formal analysis (lead); Investigation (lead); Methodology (lead); Writing – original draft (lead). **Gerhard Böhm**: Resources (equal). **Mikhail A. Belkin**: Funding acquisition (equal); Project administration (equal); Supervision (equal); Writing – review & editing (equal).

DATA AVAILABILITY

The data that support the findings of this study are available within the article.

REFERENCES

[1] Y.-C. Chang, P. Wägli, V. Paeder, A. Homsy, L. Hvozdara, P. Van Der Wal, J. Di Francesco, N. F. De Rooij, and H. Peter Herzig, Lab Chip **12**, 3020 (2012).
[2] S. Borri, G. Insero, G. Santambrogio, D. Mazzotti, F. Cappelli, I. Galli, G. Galzerano, M. Marangoni, P. Laporta, V. Di Sarno, L. Santamaria, P. Maddaloni, and P. De Natale, Appl. Phys. B **125**, 18 (2019).
[3] G. Wysocki, R. Lewicki, R. F. Curl, F. K. Tittel, L. Diehl, F. Capasso, M. Troccoli, G. Hofler, D. Bour, S. Corzine, R. Maulini, M. Giovannini, and J. Faist, Appl. Phys. B **92**, 305 (2008).
[4] T. Fortier and E. Baumann, Commun. Phys. **2**, 153 (2019).
[5] A. Hugi, G. Villares, S. Blaser, H. C. Liu, and J. Faist, Nature **492**, 229 (2012).
[6] J. Faist, G. Villares, G. Scalari, M. Rösch, C. Bonzon, A. Hugi, and M. Beck, Nanophotonics **5**, 272 (2016).
[7] L. A. Sterczewski, M. Bagheri, C. Frez, C. L. Canedy, I. Vurgaftman, M. Kim, C. S. Kim, C. D. Merritt, W. W. Bewley, and J. R. Meyer, J. Phys. Photonics **3**, 042003 (2021).
[8] B. Schwarz, J. Hillbrand, M. Beiser, A. M. Andrews, G. Strasser, H. Detz, A. Schade, R. Weih, and S. Höfling, Optica **6**, 890 (2019).
[9] Q. Y. Lu, S. Manna, S. Slivken, D. H. Wu, and M. Razeghi, AIP Adv. **7**, 045313 (2017).
[10] Y. Okawachi, K. Saha, J. S. Levy, Y. H. Wen, M. Lipson, and A. L. Gaeta, Opt. Lett. **36**, 3398 (2011).
[11] H. J. Chen, Q. X. Ji, H. Wang, Q. F. Yang, Q. T. Cao, Q. Gong, X. Yi, and Y. F. Xiao, Nat. Commun. **11**, 2336 (2020).
[12] M. H. P. Pfeiffer, C. Herkommer, J. Liu, H. Guo, M. Karpov, E. Lucas, M. Zervas, and T. J. Kippenberg, Optica **4**, 684 (2017).
[13] B. Stern, X. Ji, Y. Okawachi, A. L. Gaeta, and M. Lipson, Nature **562**, 401 (2018).
[14] M. Yu, Y. Okawachi, A. G. Griffith, M. Lipson, and A. L. Gaeta, Optica **3**, 854 (2016).
[15] K. Luke, Y. Okawachi, M. R. E. Lamont, A. L. Gaeta, and M. Lipson, Opt. Lett. **40**, 4823 (2015).
[16] N. Singh, D. D. Hudson, Y. Yu, C. Grillet, S. D. Jackson, A. Casas-Bedoya, A. Read, P. Atanackovic, S. G. Duvall, S. Palomba, B. Luther-Davies, S. Madden, D. J. Moss, and B. J. Eggleton, Optica **2**, 797 (2015).
[17] M. Sinobad, C. Monat, B. Luther-davies, P. Ma, S. Madden, D. J. Moss, A. Mitchell, D. Allioux, R. Orobtchouk, S. Boutami, J.-M. Hartmann, J.-M. Fedeli, and C. Grillet, Optica **5**, 360 (2018).
[18] D. Martyshkin, V. Fedorov, T. Kesterson, S. Vasilyev, H. Guo, J. Liu, W. Weng, K. Vodopyanov, T. J. Kippenberg, and S. Mirov, Opt. Mater. Express **9**, 2553 (2019).
[19] K. Zhang, G. Böhm, and M. A. Belkin, Appl. Phys. Lett. **120**, 061106 (2022).
[20] S. Jung, D. Palaferri, K. Zhang, F. Xie, Y. Okuno, C. Pinzone, K. Lascola, and M. A. Belkin, Optica **6**, 1023 (2019).
[21] N. K. Hon, R. Soref, and B. Jalali, J. Appl. Phys. **110**, 011301 (2011).
[22] X. Gai, Y. Yu, B. Kuyken, P. Ma, S. J. Madden, J. Van Campenhout, P. Verheyen, G. Roelkens, R. Baets, and B. Luther-Davies, Laser Photonics Rev. **7**, 1054 (2013).
[23] T. Wang, N. Venkatram, J. Gosciniak, Y. Cui, G. Qian, W. Ji, and D. T. H. Tan, Opt. Express **21**, 32192 (2013).
[24] L. Carletti, P. Ma, Y. Yu, B. Luther-Davies, D. Hudson, C. Monat, R. Orobtchouk, S. Madden, D. J. Moss, M. Brun, S. Ortiz, P. Labeye, S. Nicoletti, and C. Grillet, Opt. Express **23**, 8261 (2015).
[25] S. Serna, V. Vakarin, J. M. Ramirez, J. Frigerio, A. Ballabio, X. Le Roux, L. Vivien, G. Isella, E. Cassan, N. Dubreuil, and D. Marris-Morini, Sci. Rep. **7**, 14692 (2017).
[26] K. Thyagarajan and A. Ghatak, "Some important nonlinear effects in optical fibers," in *Guided Wave Optical Components and Devices,* edited by B.P Pal (Elsevier Academic Press, Burlington, MA, 2006), pp. 91–100.
[27] C. Wang, M. Zhang, M. Yu, R. Zhu, H. Hu, and M. Loncar, Nat. Commun. **10**, 978 (2019).
[28] R. W. Boyd, *Nonlinear Optics*, 3rd ed. (Academic Press, Waltham, MA, 2008).
[29] T. J. Kippenberg, S. M. Spillane, and K. J. Vahala, Phys. Rev. Lett. **93**, 083904 (2004).
[30] M. H. Chou, I. Brener, M. M. Fejer, E. E. Chaban, and S. B. Christman, IEEE Photonics Technol. Lett. **11**, 653 (1999).

[31] X. Ji, F. A. S. Barbosa, S. P. Roberts, A. Dutt, J. Cardenas, Y. Okawachi, A. Bryant, A. L. Gaeta, and M. Lipson, Optica **4**, 619 (2017).
[32] F. Smektala, C. Quemard, L. Leneindre, J. Lucas, A. Barthélémy, and C. De Angelis, J. Alloys Compd. **239**, 139 (1998).
[33] W. C. Hurlbut, K. L. Vodopyanov, P. S. Kuo, M. M. Fejer, and Y. S. Lee, Opt. Lett. **32**, 668 (2007).
[34] A. Villeneuve, C. C. Yang, G. I. Stegeman, C. H. Lin, and H. H. Lin, Appl. Phys. Lett. **62**, 2465 (1993).
[35] D. C. Hutchings, J. S. Aitchison, B. S. Wherrett, G. T. Kennedy, and W. Sibbett, Opt. Lett. **20**, 991 (1995).
[36] J. Chiles, N. Nader, E. J. Stanton, D. Herman, G. Moody, J. Zhu, J. Connor Skehan, B. Guha, A. Kowligy, J. T. Gopinath, K. Srinivasan, S. A. Diddams, I. Coddington, N. R. Newbury, J. M. Shainline, S. W. Nam, and R. P. Mirin, Optica **6**, 1246 (2019).
[37] M. Sheik-Bahae and E. W. Van Stryland, "Optical nonlinearities in the transparency region of bulk semiconductors," Semicond. Semimetals **58**, 257 (1998).
[38] Y. Yu, X. Gai, P. Ma, D.-Y. Choi, Z. Yang, R. Wang, S. Debbarma, S. J. Madden, and B. Luther-Davies, Laser Photonics Rev. **8**, 792 (2014).
[39] T. R. Ensley and N. K. Bambha, Opt. Express **27**, 37940 (2019).